JOURNAL OF Materials CHEMISTRY

Rare-earth doping of nickel zinc ferrites

Rainer Hochschild* and Hartmut Fuess

FG Strukturforschung, FB Materialwissenschaft, TU-Darmstadt, Petersenstr. 23, D-64287 Darmstadt, Germany. E-mail: Rainer_Hochschild@exchange.de

Received 12th July 1999, Accepted 26th October 1999

The influence of small substitution of iron with rare-earth cations in nickel zinc ferrites has been investigated. Samples with overall composition $Ni_{0.50}Zn_{0.51}Fe_{1.96}R_{0.04}O_{4+\delta}$ (R = Pr, Nd, Eu, Ho, Tm, Lu) were prepared by a wet chemical route. The substitution of iron by rare-earth cations results in the formation of various rare-earth iron oxides in the bulk ferrite during sintering. Differences in the electrical and magnetic properties of the doped samples are interpreted on the basis of phase composition and microstructure.

1 Introduction

Soft magnetic ferrites are a key material for compact switched mode power supplies (SMPS). Miniaturization—one of the major driving forces in electronics—demands a shift to higher operating frequencies in these devices in order to satisfy the requirements of compact size and high sustained power. Due to their inherent high electrical resistivity, nickel zinc ferrites are superior to the more common manganese zinc ferrites for these applications.

In this work, the influence of small rare-earth additions on the crystal structures and properties of nickel zinc ferrites was studied. $Ni_{0.50}Zn_{0.51}Fe_2O_{4+\delta}$ was chosen as the reference composition, substituting 2 mol% iron with rare-earth elements for a final composition of $Ni_{0.50}Zn_{0.51}Fe_{1.96}R_{0.04}O_{4+\delta}$. Studies by Rezlescu *et al.*[1–3] indicate that the integration of rare-earth cations into the spinel structure of nickel zinc ferrite results in modification of basic electrical and magnetic properties. Their investigation showed a lowering of the Curie temperature and saturation magnetisation due to the substitution of iron with lanthanides, the formation of a plateau in the temperature-dependent initial permeability curve and an increase in the specific dc resistivity. Additionally, microstructural parameters like grain size and porosity were affected.

However, some of their results do not seem to be very reliable. None of their samples were single-phase, qualitative phase analysis for each sample was incomplete and no attempt at a quantitative phase analysis was made. With rare-earth substitutions adding up to only 0.67 at.% of all cations, the identification of rare-earth-containing secondary phases by X-ray powder diffraction indicates that most of the rare-earth cations are located in these secondary phases and do not enter the spinel lattice of the nickel zinc ferrite. Variations in the Fe^{2+} concentration of the samples between 1.1 and 6.8% of the total iron content could be responsible for the differences in the magnetic properties of the ferrites.

All these points were assumed to be related to their synthetic method, a classic ceramic processing route. In order to obtain more reliable results, a sophisticated wet chemical approach was chosen for syntheses in this work.

2 Experimental

Samples were prepared using two slightly different three-stage syntheses. In either case, aqueous solutions containing stoichiometric amounts of the respective metal cations were converted to metal-rich polymers by adding specific organic compounds (see appendix for further details). After slow dehydration these metalloorganic precursors were calcined in a furnace at 400 °C for 2 h. The resulting mixed oxide powders were pressed into pellets and sintered in air at 1100 °C for 10 h. See appendix for detailed descriptions of the syntheses.

Calcined and sintered samples were analysed using X-ray powder diffraction and scanning and transmission electron microscopy. In addition, the porosity of selected sintered samples was determined by mercury intrusion. Basic electrical and magnetic properties were studied using impedance spectroscopy, magnetisation and magnetic permeability measurements.

Powder diffraction data for the calcined precursors were collected on a Siemens D500 diffractometer using Cu-Kα radiation, scintillation counter and a graphite (0 0 2) secondary monochromator (Bragg–Brentano geometry). High-resolution powder diffraction measurements of the sintered ferrites were performed with a STOE STADI P diffractometer. The main setup for this instrument included a germanium (1 1 1) primary beam monochromator, Co-Kα_1 radiation and a 6° linear position sensitive detector in the STOE transmission geometry.

TEM studies were carried out with a 200 kV Philips CM 20 electron microscope and SEM images were taken using a Philips XL 30 FEG microscope.

A custom-built instrument comprising HP-4284A (20 Hz–1 MHz) and HP-4285A (75 kHz–30 MHz) LCR-meters with a pseudo 4-point layout was used for impedance spectroscopy. Sintered pellets of approx. 10 mm diameter and 1–2 mm thickness were placed between two cylindrical silver electrodes. Contacts were made using silver paint. Measurements were performed in a furnace in air between room temperature and 373 K.

Magnetisation measurements were carried out at 300 K with an Oxford Instruments Model 3001 VSM. Toroidal samples (outer diameter 28–32 mm, inner diameter 14–16 mm, thickness 2–3 mm) were used for magnetic permeability measurements (HP-4275 LCR-meter 10 kHz–10 MHz).

3 Results and discussion

3.1 Diffraction and EM-studies

The major phase in all samples already exists in the spinel structure, with minor amounts of nickel oxide and zinc oxide as secondary phases. Quantitative phase analysis was accomplished by Rietveld refinement of diffraction patterns (see Table 1). Spinel phase contents ranged from 80–95 mass% depending on the type of precursor used for synthesis. Besides phase analysis, the most important features of these measurements are the very broad diffraction peaks due to particle-size broadening. Mean crystallite sizes were calculated using the

This journal is © The Royal Society of Chemistry 2000

Table 1 Quantitative phase composition of calcined precursors (mass%) and mean particle size D of the spinel phase. The relative error for both is approx. 5%.

Series	R	Spinel	NiO	ZnO	D/nm
I	—	98	2	—	35
	Pr	94	6	—	16
	Nd	93	7	—	18
	Eu	96	3	1	23
	Ho	94	6	—	16
	Tm	95	5	—	18
	Lu	95	5	—	17
II	—	86	11	3	33
	Pr	84	11	5	13
	Nd	81	13	6	16
	Eu	82	13	5	10
	Ho	81	13	6	12
	Tm	82	13	5	14
	Lu	67	12	21	17

well-known Scherrer-formula and FWHM values corrected for instrumental broadening (see Table 1). In both series the mean crystallite size of doped samples is significantly lower than without dopant. This difference suggests a diffusion inhibition induced by rare earth cations during the formation of the mixed metal oxide.

TEM studies on doped samples from both syntheses show the homogeneous distribution of rare-earth cations among the crystallites. In the case of Series I, the particle size distribution is very narrow (see Fig. 1) and the actual chemical composition, determined by EDX analysis, is equal to the formal stoichiometric composition, considering experimental errors. For Series II, a bimodal particle size distribution is observed with the majority of small crystallites ranging from 5–9 nm and bigger ones with sizes up to 35 nm. EDX analyses for these larger crystallites show that they are essentially free of rare-earth cations, in contrast to the stoichiometric composition of the small crystallites.

After sintering, all samples consist of micrometer-sized crystallites (see Fig. 2). The mean crystallite sizes of doped samples were slightly smaller than for undoped ones. Qualitative phase analysis using X-ray powder diffraction reveals that none of the sintered samples is single-phased. Observed secondary phases include rare-earth orthoferrites $RFeO_3$ (R = Pr, Nd, Eu, Ho, Tm, Lu), so-called hexagonal ferrites RFe_2O_4 (R = Ho, Tm, Lu), mixed nickel zinc oxide and further rare-earth transition metal oxides whose structure and composition could not be determined. Quantitative phase analysis, using Rietveld refinements (see Fig. 3), of powder diffraction data shows that the fraction of spinel phase amounts up to 99% (see Table 2). Every doped sample contains one or more rare-earth iron oxides which together represent the total amount of rare-earth dopants preventing rare-earth cations from being built into the spinel structure. A direct consequence of the formation of rare-earth iron oxides is a higher iron deficiency for the remaining spinel phase, resulting in a higher fraction of nickel zinc oxide in order to compensate for the loss of trivalent cations.[4]

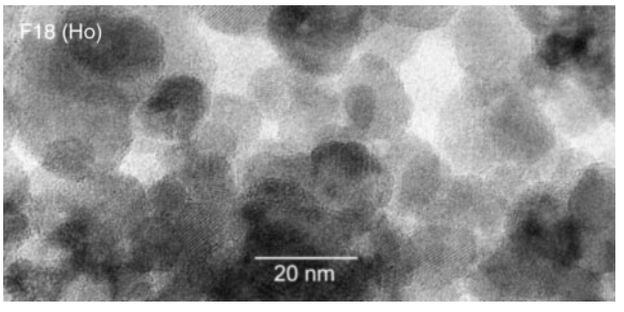

Fig. 1 TEM picture of the Ho-doped calcined precursor in series I. Mean crystallite size is approximately 16 nm.

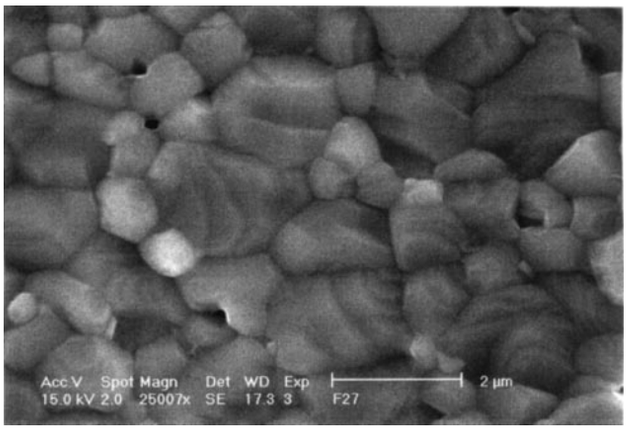

Fig. 2 SEM picture of the Lu-doped sample in series I after sintering.

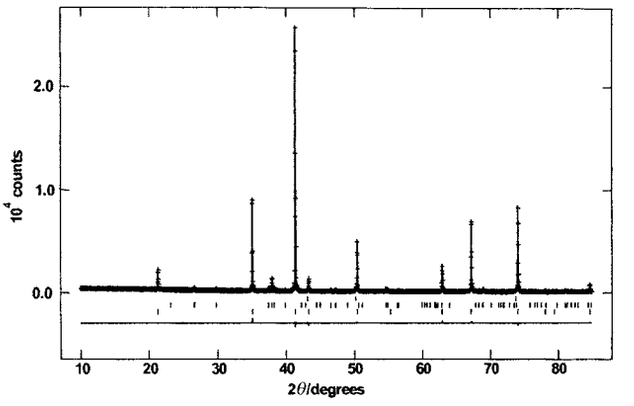

Fig. 3 Rietveld refinement of the X-ray powder diffraction pattern for the Nd-doped sintered ferrite in series II. Vertical lines mark calculated positions for Bragg reflections of $Ni_{0.5}Zn_{0.5}Fe_2O_4$, $NdFeO_3$ and NiO (bottom to top).

These findings are in contrast to previous results from Rezlescu *et al.*[1–3] who claim that at least some fraction of the rare-earth cations enter the spinel phase.

In the case of Series I, some weak diffraction peaks could not be indexed satisfactorily or assigned to known solid phases in the system R–Fe–Ni–Zn–O. However, there are strong indications that these peaks belong to rare-earth-containing phases because of systematic shifts in the corresponding d-values with varying cation size.

TEM investigations confirmed the absence of rare-earth cations in crystallites with spinel structures. In contrast to the more or less homogeneous distribution of rare-earth cations in the calcined precursors after sintering, the vast majority of these crystals contained no rare-earth cations at all. Attempts to identify those phases producing unknown diffraction peaks in Series I failed because of their low abundance.

3.2 Electric and magnetic properties

Nickel zinc ferrites belong to the group of so-called 'hopping' semiconductors. The basic process for this type of conduction is thermally activated hopping of electrons from one cation to adjacent ones. Multivalent cations, such as iron or nickel, play the key role in the conduction process for solids of this kind.

One great advantage of impedance spectroscopy compared with dc methods is the possibility of resolving conduction processes with different characteristic time constants. All dense sintered samples (porosity $<10\%$) show two slightly depressed

Table 2 Quantitative phase composition of sintered ferrites (mass%). Values in brackets denote relative composition of known phases (see text)

Series	R	Spinel	$RFeO_3$	RFe_2O_4	NiO[a]
I	—	97.5	—	—	2.5
	Pr	(94.1)	(1.9)	—	(4.0)
	Nd	(93.6)	(2.2)	—	(4.2)
	Eu	(93.5)	(2.3)	—	(4.2)
	Ho	(95.0)	—	(1.7)	(3.3)
	Tm	(94.6)	—	(2.2)	(3.2)
	Lu	(95.5)	—	(3.1)	(1.4)
II	—	99.5	—	—	0.5
	Pr	94.7	3.7	—	1.6
	Nd	95.3	3.3	—	1.4
	Eu	95.7	2.9	—	1.4
	Ho	93.4	5.1	—	1.5
	Tm	(95.1)	(3.8)	—	(1.1)
	Lu	(97.5)	—	—	(2.5)

[a]Nickel oxide contains zinc to some extent.

arcs in the R–X-plane (see Fig. 4), which can be related to two different processes.

For analysis, experimental data was fitted against a Voigt-type model circuit consisting of two RC-loops. Really good agreement between observed and calculated data could only be achieved by replacing the ideal capacitors with so-called constant phase elements.

The dispersion at high frequencies (starting in the origin in this plot) is caused by the bulk conduction process. The related capacity is equivalent to the geometric capacity of the arrangement (about 10^{-11} F). The low-frequency dispersion is caused by conduction across grain boundaries having a much higher capacity of about 10^{-8} F.

In the investigated temperature range (300–373 K), all samples exhibit Arrhenius-type temperature-dependent specific conduction of the form $\sigma = Ae^{-W/kT}$ with the activation energy, W, being controlled by charge carrier mobility (charge carrier concentration is assumed to be constant for these materials over a small temperature range[5]). After evaluating the activation energies for each process (see Table 3) the results were interpreted in terms of the partial blocking model of Bauerle,[6,7] since there is no significant difference between the activation energies of bulk conduction and conduction across grain boundaries. The observed values compare well with results from other authors.[8,9] Although no thermopower measurements were carried out, it is assumed that hole conduction dominates in these samples. The relatively high activation energy of 0.5 eV and the iron deficiency of the spinel phase both support this assumption.

Three doped samples in series II (R = Pr, Nd, Eu), possessing a high porosity (>15%), exhibited three dispersions in the R–X-plane and will not be covered in this paper.

Saturation magnetisation data are listed in Table 4. Differences between samples are mainly caused by varying spinel fractions, since the magnetic ordering of all identified secondary phases is either antiferromagnetic or paramagnetic at 300 K. Therefore, undoped samples have the highest saturation magnetisation, comparable to values published previously.[8,10]

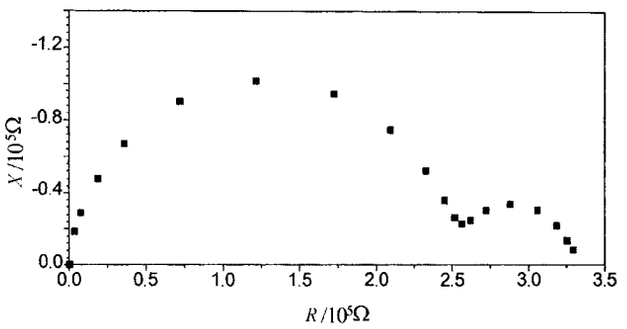

Fig. 4 Impedance spectrum of the Eu-doped sample in series I.

Table 3 Specific dc-resistivity at 300 K and activation energies for bulk and grain boundary conduction. The absolute error for these values is about 0.03 eV

Series	R	ρ_{tot}/Ω cm	W_{bulk}/eV	W_{gb}/eV	W_{bulk}/W_{gb}
I	—	1.8×10^8	0.47	0.58	0.80[a]
	Pr	5.1×10^7	0.52	0.54	0.96
	Nd	3.7×10^7	0.53	0.49	1.09
	Eu	2.9×10^7	0.52	0.49	1.06
	Ho	5.0×10^7	0.52	0.52	1.01
	Tm	3.2×10^7	0.52	0.50	1.04
	Lu	7.6×10^7	0.53	0.55	0.97
II	—	8.6×10^7	0.42	0.44	0.95
	Ho	1.6×10^8	0.46	0.56	0.81[a]
	Tm	8.4×10^7	0.52	0.56	0.93
	Lu	5.0×10^7	0.50	0.54	0.93

[a]Samples do not correspond to the partial blocking model.

Table 4 Saturation magnetization (emu g^{-1}) at 300 K and 1 T

R	Series I	Series II
—	71	70
Pr	61	65
Nd	68	65
Eu	60	67
Ho	64	69
Tm	68	64
Lu	62	54

In contrast to these measurements, permeability spectra are much more sensitive to different dopants. This effect is not caused by the integration of rare-earth cations into the spinel structure, but due to the different development of the microstructure during sintering. One piece of evidence for this hypothesis is that the lowest observed permeability values are those for the samples with the highest porosity (R = Pr, Nd, Eu in Series II). The influence of porosity and non-magnetic grain boundary layers has been the subject of work by other authors.[11,12] In both cases, the effective measured permeability is lowered because of internal demagnetising fields.

Nevertheless, the addition of rare-earth cations improves permeability in the frequency range above 1 MHz. However, this effect originates from the smaller mean crystallite size of the doped samples after sintering. The crystallites are assumed to be single-domain particles due to their small size.[13] Therefore, the dominating magnetisation mechanism will be rotational reorientation, resulting in better high-frequency properties if the low-frequency permeability is smaller. A very broad discussion covering these matters can be found in ref. 14.

4 Conclusion

The main results of this investigation can be summarized as follows: the synthesis of doped nanocrystalline ferrites from metalloorganic precursors was successful. Depending on the type of precursor used, narrow particle size distributions and a very homogeneous distribution of the rare-earth cations in the mixed metal oxide were achieved. During sintering all rare-earth additions form various secondary phases, preferentially rare-earth iron oxides. Rare-earth cations could not be detected in the spinel phase of the final ferrite. Hence, it follows that all observed changes in magnetic properties compared to undoped samples have to be interpreted in terms of spinel phase content/composition and different microstructural parameters. They are not a consequence of complex rare-earth–transition metal–interactions in the spinel lattice.

Acknowledgements

The authors are grateful to Dr. Miehe for taking the TEM figures. Support of the work by the Deutsche Forschungsgemeinschaft, reference Fu 125/25-1, and the Fonds der Chemischen Industrie is acknowledged.

Appendix

Stoichiometric amounts of zinc oxide (0.0255 mol), nickel hydroxide (0.025 mol) and ferrous nitrate nonahydrate (0.098 mol) were dissolved in a mixture of 30 ml deionized water and 10 ml 14.4 mol l^{-1} nitric acid. Rare earth sesquioxides (0.001 mol) were dissolved separately in 1 mol l^{-1} nitric acid. After mixing both solutions, 0.3 mol citric acid and 0.3 mol butane-1,4-diol (for Series I) or 1.8 mol equivalents of poly(ethylene glycol) (Series II) were added and the solution was heated to 60–70 °C for three days. The polymer thus formed was divided into small portions and calcined in air at 400 °C for 2 h. The resulting mixed oxide powders were brownish black (Series I) to brownish red in color (Series II).

References

1 N. Rezlescu, E. Rezlescu, C. Pasnicu and M. L. Craus, *J. Phys.: Condens. Matter.*, 1994, **6**, 5707.
2 N. Rezlescu, E. Rezlescu, C. Pasnicu and M. L. Craus, *J. Magn. Magn. Mater.*, 1994, **136**, 319.
3 N. Rezlescu and E. Rezlescu, *Solid State Commun.*, 1993, **88**, 139.
4 H. Takei, H. Tokumasu, H. Rikukawa and I. Sasaki, *IEEE Trans. Magn.*, 1987, **23**, 3080.
5 M. I. Klinger and A. A. Samokhvalov, *Phys. Status Solidi B*, 1977, **79**, 9.
6 J. E. Bauerle, *J. Phys. Chem. Solids*, 1969, **30**, 2657.
7 J. R. Mcdonald, *Impedance Spectroscopy*, John Wiley & Sons, New York, 1987.
8 V. R. K. Murthy and J. Sobhanadri, *Phys. Status Solidi A*, 1976, **38**, 647.
9 S. Krupicka and P. Novák, in *Ferromagnetic Materials*, vol. 3, ed. E. P. Wohlfahrt, North Holland Publishing, Amsterdam, 1982, p. 189.
10 J. Smit and H. P. J. Wijn, *Advances in Electronics and Electron Physics*, Academic Press, New York, vol. 6, 1954.
11 H. Rikukawa, *IEEE Trans. Magn.*, 1982, **18**, 1535.
12 M. T. Johnson and E. G. Visser, *IEEE Trans. Magn.*, 1990, **26**, 2235.
13 M. T. Rekveldt, *J. Phys.* (Paris), 1977, **1**, C1.
14 J. L. Snoek, *Physica*, 1948, **14**, 207.

Paper a905583e